Capacity Loss and Antenna Array Geometry

Thibaud Gabillard, Vidhya Sridhar and Athanassios Manikas
Electrical and Electronics Engineering, Imperial College London
{t.gabillard13, vidhya.sridhar11, a.manikas}@imperial.ac.uk

***Abstract*—The impact of antenna array geometry on its ability to mitigate interference, and hence the channel capacity, is a topic that is seldom studied and is crucial for future systems that will employ large arrays. In this paper, for the worst-case scenario where interferers are located spatially close to the desired user, the "capacity loss" is defined and expressed as a function of the array geometry and propagation environment. Based on the analytical results, simulation studies of the capacity loss are presented for different array geometries and various key insights on antenna array design are highlighted.**

Notation

A, a	Scalar
$\underline{A}$, $\underline{a}$	Column vector
$\mathbb{A}$	Matrix
$(\cdot)^T$	Transpose
$(\cdot)^H$	Hermitian transpose
$\|\cdot\|$	Norm of a vector
$\mathbb{I}_N$	$N \times N$ identity matrix
$\mathbb{O}_N$	$N \times N$ matrix of zeros
$\mathcal{E}\{\cdot\}$	Expectation operator
$\mathcal{C}$	Set of complex numbers
$\mathcal{R}$	Set of real numbers

I. Introduction

Future communication systems are expected to deliver high capacity whilst operating in environments with high user density and heightened interference [1]. Towards this end, large antenna arrays are expected to play a major role in providing high levels of spatial discrimination between co-channels users and improved interference cancellation. The selection of an appropriate performance measure is key to the design of efficient antenna array receivers. In this context, it is crucial to establish a relationship between the channel capacity associated with an antenna array and the given array geometry as a function of the propagation environment, to measure and study the spatial discrimination capabilities of an array.

In the wireless communication literature, considerable research has been carried out to investigate the effect of various factors on capacity, such as the presence of interference and multipaths. Based on non parametric channel models, a number of approaches to analytically model the capacity in various environments, such as channels with high interference, indoor line-of-sight (LOS) and channels with high antenna correlation [2][3], can be obtained in the literature. In [4], using a non-parametric channel model for an indoor environment, the effect of multipath propagation on the channel capacity is studied. An analysis of the channel capacity in the presence of antenna correlation and interference is presented in [5]. In [6], utilising the Kronecker channel model, approximate spatial correlation models for specific array configurations for a clustered multiple-input multiple-output (MIMO) channel are proposed. However, for large antenna array systems that are expected to play a crucial role in future communication systems, measurement and modelling campaigns show that the underlying non parametric models become quite unsuitable and erroneous since the channel does not present rich scattering [7]. Thus, an effort to utilise parametric models to study the impact of interference becomes crucial. Towards this, in [8], using 2D ray models, the channel is parametrically modelled and the effect of antenna spacing on the channel capacity is studied, albeit for a simple 2×2 MIMO system. In [9], the effect of spatial correlation on the channel capacity is studied. However, the influence of the array geometry has been ignored in the aforementioned research. There has been some research that studies the influence of array geometry on the array detection, resolution [10] and the average error of DOA estimation [11]. In [12], the impact of four uniform array geometries on the ergodic capacity in a microcellular urban environment is studied, albeit in the absence of interference. In [13] and [14], an analysis of the achievable capacity for two different sets of array geometries is estimated assuming the users are located uniformly within a sphere and a circle of known radius respectively. However, this scenario is representative of the average capacity rather than the worst case capacity that is obtained when the users are spatially very close to each other as expected in future dense urban environments. Thus, in this paper, using the novel concept of "capacity loss", a study of the impact of the array geometry on the channel capacity, with the worst case scenario of spatially close users, is studied, to address this gap in the literature.

This paper is organised as follows. In Section II, the concept of capacity loss, that occurs as a result of closely spaced interfering users, is introduced. Subsequently, in Section III, the basic differential geometry parameters to study the array

manifold are presented. This is followed by Section IV where a closed form expression of the capacity loss is obtained. In Section V, various common array geometries are compared using the capacity loss of a performance metric and various insights provided by this metric are highlighted. Finally, the paper is concluded in Section VI.

II. Capacity Loss

Consider an N-element antenna array lying on the x-y plane and operating in the presence of M users. Without any loss of generality, it is assumed that the first user is the desired user and the remaining $M-1$ are co-channel interferers with all M users located also on the x-y plane. The signal $\underline{x}(t) \in \mathcal{C}^{N\times 1}$ received by the antenna array is given as follows

$$\underline{x}(t) = \underline{\mathrm{a}}\left(\theta_1\right) m_1(t) + \sum_{i=2}^{M} \underline{\mathrm{a}}\left(\theta_i\right) m_i(t) + \underline{\mathrm{n}}(t), \qquad (1)$$

where $\underline{\mathrm{a}}\left(\theta_i\right) \in \mathcal{C}^{N\times 1}$ is the array manifold vector of the i-th user and is given as a function of the array geometry as

$$\underline{\mathrm{a}}\left(\theta_i\right) = \exp\left(-\mathrm{j}\pi\left(\underline{r}_x \cos\theta_i + \underline{r}_y \sin\theta_i\right)\right). \qquad (2)$$

In Eq. 2 the matrix $\left[\underline{r}_x, \underline{r}_y\right] \in \mathcal{R}^{N\times 2}$ represents the x and y Cartesian coordinates of the antenna array (in units of half-wavelength) and θ_i denotes the azimuth angle of the i-th source (measured anticlockwise with respect to the positive x-axis). Furthermore, in Eq. 1, $m_i(t)$ is the received baseband message signal of the i-th user, while $\underline{\mathrm{n}}(t)$ is the additive isotropic white Gaussian noise vector of zero mean and covariance $\sigma_{\mathrm{n}}^2\mathbb{I}_N$. Assuming that the M signals are uncorrelated, the covariance matrix $\mathbb{R}_{xx} \in \mathcal{C}^{N\times N}$ of the signal $\underline{x}(t)$ given by Eq. 1 is

$$\mathbb{R}_{xx} = \mathcal{E}\left\{\underline{x}(t)\underline{x}(t)^H\right\} = \sum_{i=1}^{M} P_i \underline{\mathrm{a}}\left(\theta_i\right) \underline{\mathrm{a}}^H\left(\theta_i\right) + \sigma_{\mathrm{n}}^2\mathbb{I}_N, \quad (3)$$

where P_i represents the received power of the i-th user. In this case, the channel capacity C is formally defined as the maximum of the mutual information $\mathcal{I}$ between the transmitted desired signal $m_1(t)$ and the signal received at the output of the antenna array $\underline{x}(t)$, assuming perfect knowledge of the desired array manifold vector $\underline{\mathrm{a}}(\theta_1)$. That is,

$$C = \max_{m_1} \mathcal{I}\left\{m_1(t); \underline{x}(t) \left| \underline{\mathrm{a}}(\theta_1)\right.\right\}. \qquad (4)$$

It can be shown that the channel capacity given by Eq. 4 can be written as follows

$$C = B\log_2\left(\frac{\det\left(\mathbb{R}_{xx}\right)}{\det\left(\mathbb{R}_{xx} - P_1\underline{\mathrm{a}}(\theta_1)\underline{\mathrm{a}}^H(\theta_1)\right)}\right) \text{ bits/sec}, \quad (5)$$

where B is the channel bandwidth. By defining the matrix $\mathbb{A}$ as follows

$$\mathbb{A} \triangleq \left[\underline{\mathrm{a}}\left(\theta_2\right), \ldots, \underline{\mathrm{a}}\left(\theta_M\right)\right] \in \mathcal{C}^{N\times(M-1)}, \qquad (6)$$

Eq. 5 can be rewritten as

$$C = B\log_2\left(\frac{\det\begin{bmatrix} N+\sigma_{\mathrm{n}}^2, & \sqrt{P_1}\underline{\mathrm{a}}^H(\theta_1)\mathbb{A}\mathbb{P} \\ \sqrt{P_1}\mathbb{P}\mathbb{A}^H\underline{\mathrm{a}}(\theta_1), & \mathbb{P}\mathbb{A}^H\mathbb{A}\mathbb{P} + \sigma_{\mathrm{n}}^2\mathbb{I}_{M-1}\end{bmatrix}}{\sigma_{\mathrm{n}}^2\det\left(\mathbb{P}\mathbb{A}^H\mathbb{A}\mathbb{P} + \sigma_{\mathrm{n}}^2\mathbb{I}_{M-1}\right)}\right), \qquad (7)$$

where $\mathbb{P}$ is the matrix of signal power given by

$$\mathbb{P} = \begin{bmatrix} \sqrt{P_2}, & 0, & \cdots & 0 \\ 0, & \sqrt{P_3}, & \cdots & 0 \\ \vdots & \vdots & \ddots & \vdots \\ 0, & 0, & \cdots & \sqrt{P_M}\end{bmatrix} \in \mathcal{C}^{(M-1)\times(M-1)}. \quad (8)$$

The difference between the capacity in the presence of co-channel interference, given by Eq. 7, and the capacity in the absence of interference is defined as the "capacity loss". This capacity loss denoted by C_{loss} is the negative contribution of the $M-1$ interferers in diminishing the capacity and is given as follows

$$C_{\mathrm{loss}} = -\log_2\left(1 - \frac{\underline{b}^H\mathbb{D}^{-1}\underline{b}}{N+\sigma_{\mathrm{n}}^2}\right) \text{ bits/sec/Hz}, \qquad (9)$$

where

$$\underline{b} = \sqrt{P_1}\mathbb{P}\mathbb{A}^H\underline{\mathrm{a}}\left(\theta_1\right), \qquad (10)$$

$$\mathbb{D} = \mathbb{P}\mathbb{A}^H\mathbb{A}\mathbb{P} + \sigma_{\mathrm{n}}^2\mathbb{I}_{M-1}. \qquad (11)$$

It can be noted that the absence of interferences $\mathbb{P} = \mathbb{O}_{M-1}$, which implies that the capacity loss is equal to 0 bits/sec/Hz. More importantly, this term is negligible when the interferers are spatially far away from the desired user. However, if the interfering sources are spatially close to the desired user, (as this is expected with high probability in future high density communications) the capacity loss is expected to be significant. Hence, a study of the variation in C_{loss} in terms of the array geometry can present key insights that would be crucial for the design of future systems. This forms the motivation of this paper. Please note that, as per our knowledge, the measure of "capacity loss" is introduced and studied as a function of the array geometry for the first time in this paper.

III. Parameters of the Array Manifold

In Section II, the capacity loss due to the presence of co-channel interferers that are spatially close to the desired user was introduced. However, in order to analyse the capacity loss in terms of the array geometry, it is essential to employ accurate measures to describe the shape and characteristics of the array manifold. The array manifold is defined as the locus of all the array manifold vectors $\underline{\mathrm{a}}\left(\theta\right), \forall\theta$ and is a curve $\mathcal{A}$ which is embedded in an N-dimensional complex observation space [11] and defined as

$$\mathcal{A} \triangleq \left\{\underline{\mathrm{a}}\left(\theta\right), \forall\theta \in [0^\circ, 360^\circ]\right\}. \qquad (12)$$

Since the array manifold is a function of a single parameter namely the azimuth angle θ, given by Eq. 2, all the users lie on the manifold curve $\mathcal{A}$, which in this case is also known as the θ-curve [11].

It is clear from Eq. 12 that the array manifold is conventionally parameterized in terms of the azimuth angle θ. However, parameterization in terms of the arc length s, which is the most basic feature of a curve and a natural parameter representing the actual physical length of a segment of the manifold curve, is more suitable. The arc length $s(\theta)$ along the manifold curve $\mathcal{A}$ is formally defined [11] as

$$s(\theta) \triangleq \int_0^{\theta} \left\| \frac{d\underline{\mathrm{a}}(\theta)}{d\theta} \right\| d\theta. \tag{13}$$

Figure 1 illustrates the manifold curve embedded in $\mathcal{C}^N$. It also shows the manifold vector of the desired user $\underline{\mathrm{a}}(\theta_1)$ ending at the point $s_1 \triangleq s(\theta_1)$ on the curve. The cluster of $(M-1)$ cochannel interferences is between the points $s_2 \triangleq s(\theta_2)$ and $s_M \triangleq s(\theta_M)$ on the manifold curve (shown in Fig. 1), with these two points corresponding to the manifold vectors $\underline{\mathrm{a}}(\theta_2)$ and $\underline{\mathrm{a}}(\theta_M)$ $(\theta_1 < \theta_2 < \ldots < \theta_M)$. This implies that the desired signal is outside the cluster of $(M-1)$ interferences and the closest interference is the one with direction of arrival θ_2. Furthermore, in order to facilitate the analysis of the relationship between the capacity loss and the array geometry, from here onwards, we represent the manifold vector of the i-th user $\underline{\mathrm{a}}_i$ in terms of the arc length rather than the azimuth as follows

$$\underline{\mathrm{a}}_i \triangleq \underline{\mathrm{a}}(s_i). \tag{14}$$

Thus, using this, we may define the principal curvature at any point s [11] on the array manifold $\kappa_1(s)$ as

$$\begin{aligned} \kappa_1(s) &= \left\| \frac{d^2\underline{\mathrm{a}}(s)}{ds^2} \right\| \\ &= \frac{1}{\|\dot{\underline{r}}(\theta)\|^2} \left\| \ddot{\underline{r}}(\theta) + \frac{\mathrm{j}}{\pi} \mathbb{P}^{\perp}_{\dot{\underline{r}}(\theta)} \underline{r}(\theta) \right\|, \end{aligned} \tag{15}$$

where

$$\underline{r}(\theta) = \underline{r}_x \cos\theta + \underline{r}_y \sin\theta, \tag{16}$$

$$\dot{\underline{r}}(\theta) \triangleq \frac{\partial \underline{r}(\theta)}{\partial\theta} = -\underline{r}_x \sin\theta + \underline{r}_y \cos\theta \tag{17}$$

and $\mathbb{P}^{\perp}_{\dot{\underline{r}}(\theta)}$ represents the complement projection operator onto the subspace spanned by $\dot{\underline{r}}(\theta)$. That is,

$$\mathbb{P}^{\perp}_{\dot{\underline{r}}(\theta)} = \mathbb{I}_N - \dot{\underline{r}}(\theta) \left(\dot{\underline{r}}^H(\theta) \dot{\underline{r}}(\theta) \right)^{-1} \dot{\underline{r}}^H(\theta). \tag{18}$$

In particular, using Eq. 15 we may find the principal curvature $\kappa_1(s_c)$ at the centre of the cluster of the interfering

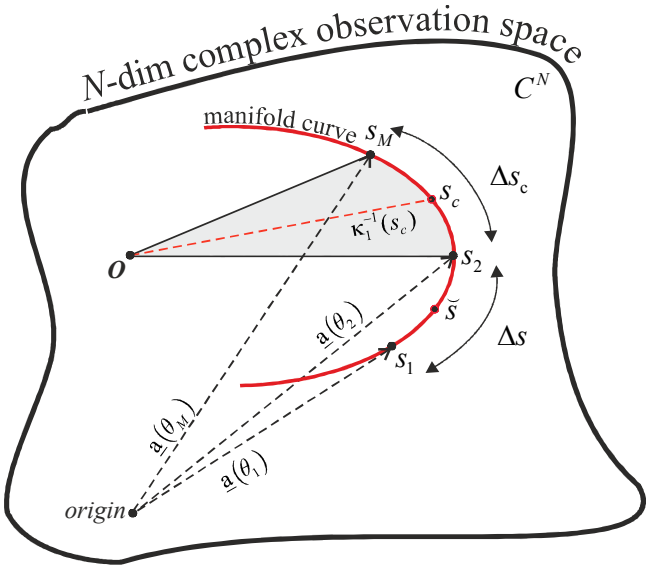

Fig. 1. Representation of the array manifold vectors of the desired user $\underline{\mathrm{a}}_1$ and interferers $\underline{\mathrm{a}}_2, \ldots, \underline{\mathrm{a}}_M$ on the array manifold curve $\mathcal{A}$. The arclength between the closest interferer and the desired user is assumed to be Δs while the cluster size of interference is Δs_c. The point O denotes the centre of curvature of the arc on which the interferer cluster lies with radius equal to $\kappa_1(s_c)$.

users, i.e. at point s_c given by

$$s_c \triangleq s(\theta_c) = \frac{(s_2 + s_M)}{2}. \tag{19}$$

The parameter s_c is shown in Fig. 1 together with $\Delta s_c = s_M - s_2$ which is the arc length of the cluster and corresponds to an angular separation $\Delta\theta_c = \theta_M - \theta_2$. Assuming a circular approximation[1] of the manifold curve in the region of the cluster, the radius of this segment is the inverse of the principal curvature $\kappa_1^{-1}(s_c)$ as also shown in Fig. 1. In this case, we may express the inner product between two array manifold vectors $\underline{\mathrm{a}}(s_i)$ and $\underline{\mathrm{a}}(s_j)$ in the cluster as

$$\underline{\mathrm{a}}^H(s_i)\,\underline{\mathrm{a}}(s_j) \approx N - 2\kappa_1^{-2}(s_c) \sin^2\left(\frac{(j-i)\Delta s_c}{(M-2)\,2\kappa_1^{-1}(s_c)} \right) \tag{20}$$

with $2 \le i, j \le M$.

The above definitions and concepts will be utilised in the next section to analyse the relationship between the capacity loss and the array geometry.

IV. Capacity Loss and the Array Manifold

In this section, the capacity loss defined in Section II is expressed as functions of arc lengths and first curvature of the array manifold defined in Section III. The desired user and the $M-1$ remaining interferers are denoted by their corresponding array manifold vectors $\underline{\mathrm{a}}_1$ and $\underline{\mathrm{a}}_2, \ldots, \underline{\mathrm{a}}_M$ respectively. The

[1]For larger Δs_c, corresponding to larger $\Delta\theta_c$, the circular approximation may not be valid and the second curvature $\kappa_2(s_c)$ of the array manifold curve may need to be calculated and used.

impinging angle of the desired user is θ_1 while the $M-1$ interferers have angles of $\theta_2, \ldots, \theta_M$ respectively. Recalling Fig. 1 that describes the array environment, we assume that the angular separation between the desired user and the cluster of interferences is small enough to result in a capacity loss. For the sake of simplicity, we assume that the desired user and all interferers are received with unity power. That is, $P_1 = P_2 = \ldots = P_M = 1$. Recalling Eq. 9, the matrix $\mathbb{D} \in \mathcal{C}^{(M-1)\times(M-1)}$ may be expressed as follows

$$\mathbb{D} = \begin{bmatrix} \underline{a}_2^H \underline{a}_2, & \underline{a}_2^H \underline{a}_3, & \ldots & \underline{a}_2^H \underline{a}_M \\ \underline{a}_3^H \underline{a}_2, & \underline{a}_3^H \underline{a}_3, & \ldots & \underline{a}_3^H \underline{a}_M \\ \vdots & \vdots & \ddots & \vdots \\ \underline{a}_M^H \underline{a}_2, & \underline{a}_M^H \underline{a}_3, & \ldots & \underline{a}_M^H \underline{a}_M \end{bmatrix} + \sigma_{\mathrm{n}}^2 \mathbb{I}_{M-1}. \quad (21)$$

Consequently, $\mathbb{D}$ can be expressed in terms of the array manifold parameters introduced in Section III as follows

$$\mathbb{D} \approx -2\kappa_1^{-2}(s_{\mathrm{c}}) \sin^2\left(\mathbb{M} \frac{\Delta s_{\mathrm{c}}}{2\kappa_1^{-1}(s_{\mathrm{c}})(M-2)}\right) \quad (22)$$

$$+ N\underline{1}_{M-1}\underline{1}_{M-1}^T + \sigma_{\mathrm{n}}^2 \mathbb{I}_{M-1}, \quad (23)$$

where $\mathbb{M}$ is the following Toeplitz matrix

$$\mathbb{M} \triangleq \begin{bmatrix} 0, & 1, & \ldots & M-2, \\ 1, & 0, & \ldots & M-1, \\ \vdots & \vdots & \ddots & \vdots \\ M-2, & M-1, & \ldots & 0 \end{bmatrix}. \quad (24)$$

Remember that, s_{c} denotes the centre of the interferer cluster (see Fig. 1) and $\kappa_1(s_{\mathrm{c}})$ is given by Eq. 15. In a similar fashion, $\underline{b}$ in Eq. 9 may be written as

$$\underline{b} = \begin{bmatrix} \underline{a}_1^H \underline{a}_2 \\ \underline{a}_1^H \underline{a}_3 \\ \vdots \\ \underline{a}_1^H \underline{a}_M \end{bmatrix} \in \mathcal{C}^{(M-1)\times 1}, \quad (25)$$

which may be, in turn, expressed in terms of the array manifold parameters as follows

$$\underline{b} \approx N\underline{1}_{M-1} - 2\kappa_1^{-2}(\breve{s}) \quad (26)$$

$$\times \sin^2\left(\left(\Delta s \underline{1}_{M-1} + \frac{\Delta s_{\mathrm{c}}}{(M-2)} \mathbb{M} \begin{bmatrix} 1 \\ \underline{0}_{M-2} \end{bmatrix}\right) \frac{1}{2\kappa_1^{-1}(\breve{s})}\right), \quad (27)$$

where $\breve{s}$ is the centre of $\Delta s = s_2 - s_1$, i.e.

$$\breve{s} = \frac{s_1 + s_2}{2}. \quad (28)$$

Equation 9, in conjunction with Eqs. 22 and 26, establish an important relationship between the capacity loss and the most important parameters of the array manifold, namely the arc length and the principal curvature which are, in turn, dictated by the array geometry and the propagation environment. This is a crucial design equation for antenna arrays and will be investigated for different array geometries in the next section.

V. Computer Simulation Studies

In order to study the impact of the array manifold parameters on the capacity loss, given by Eq. 9, two sets of five array geometries were studied. In the first set, all five geometries have the same number of antennas N but different aperture. In the second set, all five geometries have approximately the same aperture but different number of antenna elements. A half-wavelength inter-antenna spacing was maintained across both sets of geometries. All the geometries belong to the class of "2D grid arrays" [11] which are defined as the geometries which satisfy the following conditions:

$$\underline{r}_x^T \underline{r}_y = 0 \text{ and } \|\underline{r}_x\| = \|\underline{r}_y\|. \quad (29)$$

A. Array Geometries with Equal Number of Antennas

All the 2D grid arrays considered in this subsection have 24 antennas as shown in Fig. 2. Furthermore, the propagation environment was assumed to be composed of one desired user and three interferers. The Δs_{c} was set such as the cluster of interfering users is set to 3°. That is, $\Delta\theta_{\mathrm{c}} = 3^\circ$. In addition, the Δs was set such as the angular separation $\Delta\theta_{1,2}$ was varied between 0° and 7°. For this environment, the resulting capacity loss for the five geometries is also illustrated in Fig. 2 with variable $\Delta\theta_{1,2}$ and variable θ_1.

As mentioned in Section IV, the arc length and principal curvature are two crucial array manifold parameters that contribute to the capacity loss. For the case of grid arrays [11], the length of the arc Δs is given by

$$\Delta s = \pi \|\underline{r}_x\| \Delta\theta_{1,2}, \quad (30)$$

and, hence, is constant over the θ-curve for a fixed value of $\Delta\theta_{1,2}$ while increases linearly with $\Delta\theta_{1,2}$. In Fig. 2, this, in conjunction with Eq. 9, explains the decrease of C_{loss} with increased $\Delta\theta_{1,2}$.

Equations 9, 22 and 26 indicate that there exists a trade-off between the array aperture, curvature and number of antennas, that will enable the minimisation of capacity loss. In the chosen geometries, with fixed N, the influence of Δs given by Eq. 30 is high. This explains the ranking of geometries in Table I where the Circular array yields the lowest capacity loss, since it possesses the highest value of $\|\underline{r}_x\|$, and the "Filled"-grid provides the highest capacity loss, since it possesses the lowest value of $\|\underline{r}_x\|$. Table I also gives the the total length of the manifold of each of the array geometries with $N = 24$ antennas. Using the rule that "the best array geometry is the one which provides the smallest C_{loss} for a given $\Delta\theta_{1,2}$", the best geometry in Fig. 2 is the Circular geometry. The same ranking results also by observing the capacity loss graphs shown in Fig. 2.

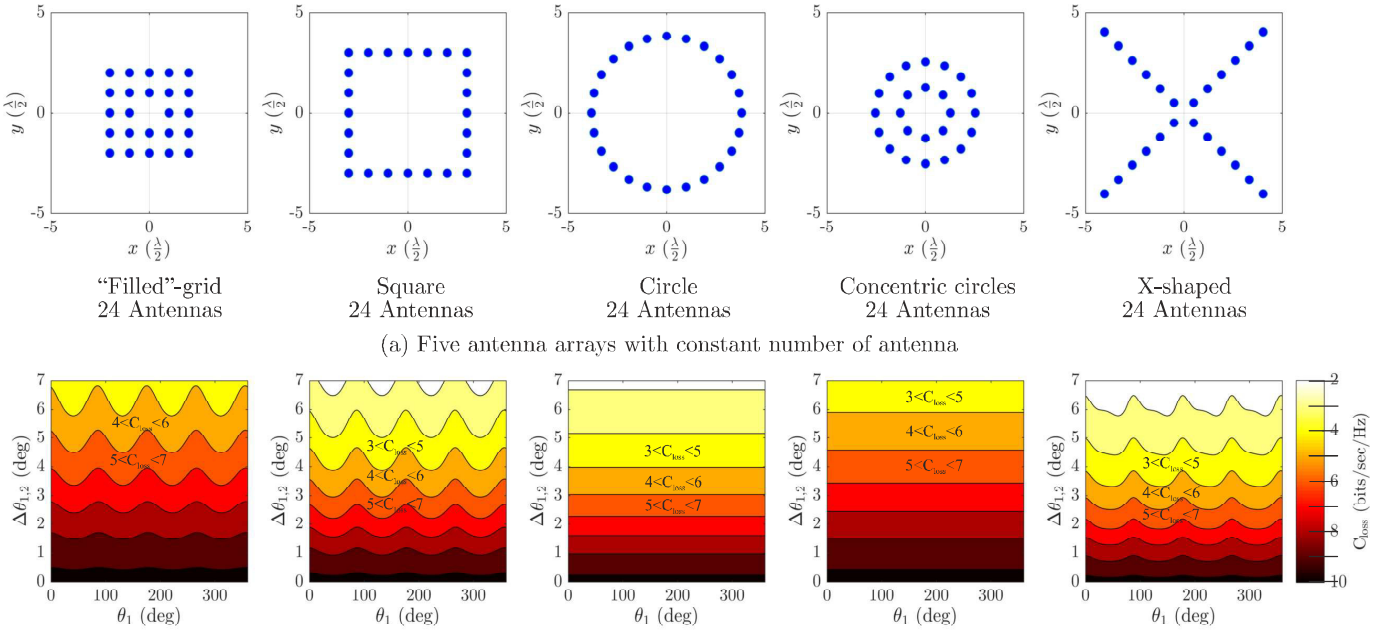

(a) Five antenna arrays with constant number of antenna

(b) Capacity loss C_{loss} for varying azimuth θ_1 and separation $\Delta\theta_{1,2}$ between the interfering cluster and desired user.

Fig. 2. Five antenna arrays with constant number of antennas namely (a) "filled"-grid, (b) square, (c) circle, (d) concentric circle and (e) X-shaped. The performance of each array geometry was evaluated in terms of the capacity loss with varying θ_1 and $\Delta\theta_{1,2}$ and are presented below the illustration of the corresponding array geometry.

TABLE I
COMPARISON (RANKING) OF THE TWO SETS OF FIVE ARRAY GEOMETRIES BASED ON THE CAPACITY LOSS.

	Fixed Number of Antennas ($N = 24$)			Equal Aperture		
Array geometry	$\|\underline{r}_x\| = \|\underline{r}_y\|$	Manifold length ℓ_m	Ranking	$\|\underline{r}_x\|$	Manifold length ℓ_m	Ranking
"Filled"-grid	7.07	139.58	last	14	276.35	4th
Square	12.08	238.51	3rd	12.08	238.51	2nd
Circle	13.23	261.19	best	9	177.65	3rd
Concentric circles	7.64	150.80	4th	9.68	191.04	last
X-shaped	12.59	248.45	2nd	8.22	162.17	best

Note that, in this case, it is the norm $\|\underline{r}_x\|$ $\left(= \|\underline{r}_y\|\right)$ of the array geometry that matters more than the array aperture. Furthermore, when the value of $\|\underline{r}_x\|$ increases, the impact of the principal curvature κ_1 is magnified and this results in an increase in the capacity loss.

B. Array Geometries with Approximately Equal Aperture

In this subsection, 2D grid arrays of the same aperture are investigated. Figures 3a and 3b illustrate the array geometries and their corresponding capacity losses for the same environment as described in Section V-A. Table I gives the performance ranking of the geometries shown in Fig. 3. An interesting result is that the "Square" array and X-shaped array yield a result very similar to that of the "Filled"-grid array even though the "Filled"-grid has a higher number of antennas. This can be explained by applying the result obtained in Eq. 9 for this set of geometries. Unlike the geometries in Fig. 2, the geometries in Fig. 3 have different number of antennas. This implies that there is now an interplay between three different parameters namely $\|\underline{r}_x\|$, κ_1 and N that results in the ranking given in Table I. The relationship between these parameters dictates the performance ranking.

Figure 5 illustrates the variation in capacity loss for the arrays shown in Fig. 3 but with varying number of users M. As before, the interferer cluster is 3° and, the desired user is fixed at $\theta_1 = 20°$. The separation $\Delta s = s_2 - s_1$ between the desired user and the second user (closest interference) is set such as $\Delta\theta_{1,2} = 6°$.

Finally, consider the scenario where the desired user is located at the center of a cluster of 4 interferers (i.e. $M = 5$) with $\Delta\theta_c = 3°$. The DOA of the desired user θ_1 is variable and this is horizontal axis in Fig. 4 which illustrates the capacity loss for the geometries shown in Fig. 3. It can be observed that the capacity loss is approximately the same for all geometries

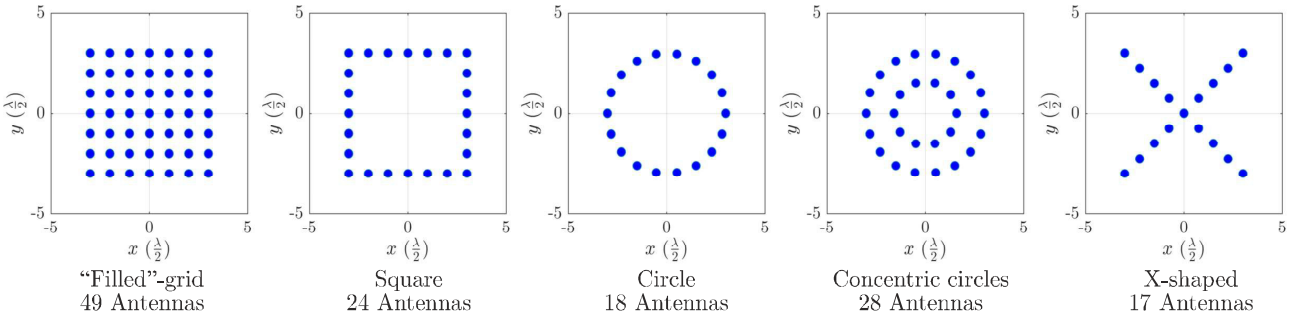

(a) Five antenna arrays with constant aperture.

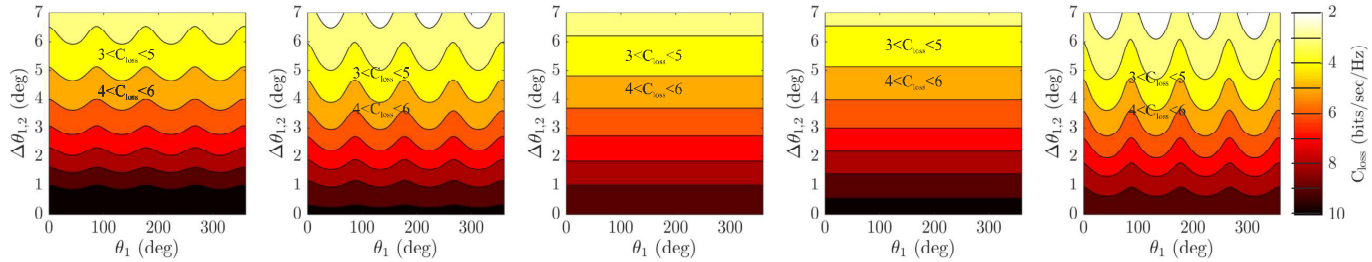

(b) Capacity loss C_{loss} for varying azimuth θ_1 and separation $\Delta\theta_{1,2}$ between the interfering cluster and desired user.

Fig. 3. Five antenna arrays with constant aperture namely (a) "filled"-grid, (b) square, (c) circle, (d) concentric circle and (e) X-shaped. The performance of each array geometry was evaluated in terms of the capacity loss with varying θ_1 (corresponding to s_1) and $\Delta\theta_{1,2}$ (corresponding to Δs) and are presented below the illustration of the corresponding array geometry.

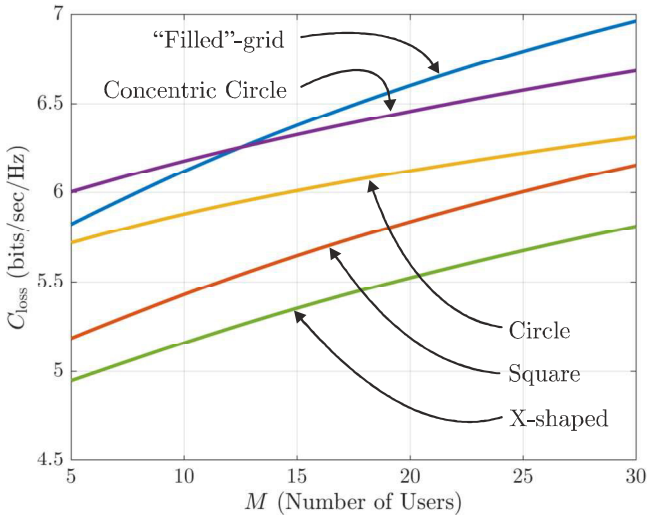

Fig. 5. Capacity loss with varying number of users M for the geometries in Fig. 3. The parameters utilised are $\theta_1 = 20°$ and $\Delta\theta_{1,2} = 6°$ with the $M-1$ interferers distributed within a Δs_c, which corresponds to $\Delta\theta_c = 3°$.

although the small difference in capacity loss is dictated by the number of antennas N.

Overall, the results of Sections V-A and V-B, highlight the importance of the "capacity loss" derived in Eq. 9. This expression can be utilised as a cost function to be optimized for future array design algorithms especially for propagation environments where high user density needs to be tackled.

VI. Conclusion

In this paper, in order to study the impact of heightened interference in future dense networks, the channel capacity for the scenario of interferers closely spaced to the desired user was analysed. In this context, the concept of "capacity loss" was introduced and expressed in terms of the array geometry and the propagation environment. The analytical results were supported by simulations studies, where it was demonstrated that in highly dense networks, array manifold parameters, such as the arc length and principal curvature, play a major role in the mitigation of interferences. The capacity loss metric derived in this paper can be utilised as a crucial tool for array design.

References

[1] N. Bhushan, D. Malladi, R. Gilmore, D. Brenner, A. Damnjanovic, R. Sukhavasi, C. Patel, and S. Geirhofer, "Network densification: the dominant theme for wireless evolution into 5G," *IEEE Communications Magazine*, vol. 52, pp. 82–89, Feb. 2014.

[2] R. Liu, R. Ying, and G. Xu, "The ultimate capacity of MIMO channels and its realization," in *18th IEEE European Conference on Circuit Theory and Design*, pp. 695–698, Aug. 2007.

[3] C. H. Y. Eugene, K. Sakaguchi, and K. Araki, "Experimental and analytical investigation of MIMO channel capacity in an indoor line-of-sight (LOS) environment," in *15th IEEE International Symposium on Personal, Indoor and Mobile Radio Communications*, vol. 1, pp. 295–300, Sept. 2004.

[4] K. I. Ziri-Castro, W. G. Scanlon, and N. E. Evans, "Prediction of variation in MIMO channel capacity for the populated indoor environment using a radar cross-section-based pedestrian model," *IEEE Transactions on Wireless Communications*, vol. 4, pp. 1186–1194, May 2005.

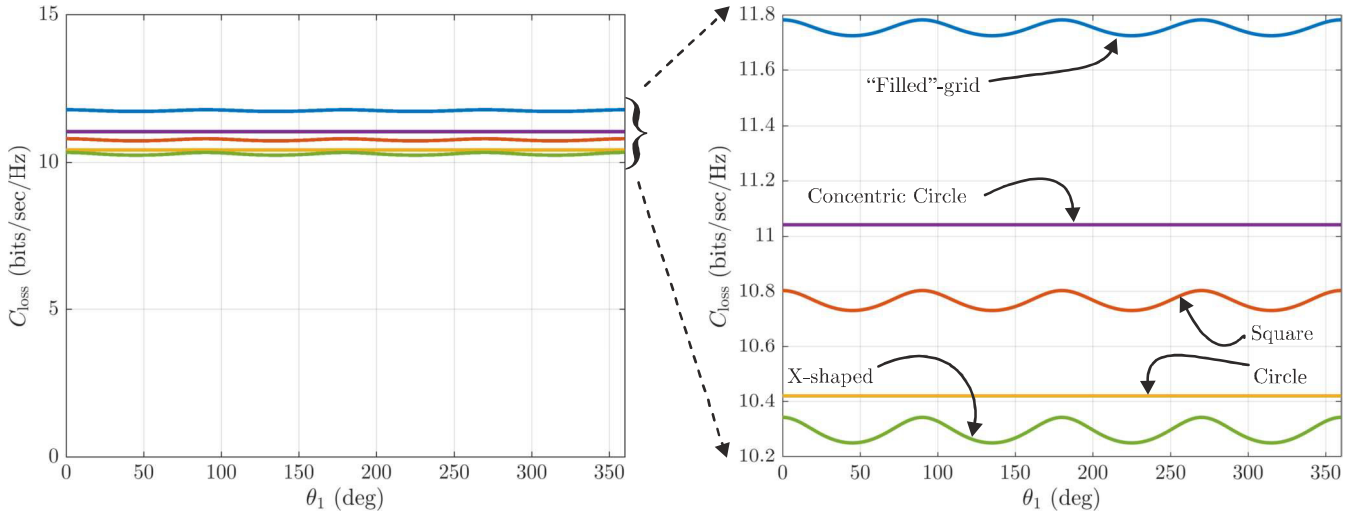

Fig. 4. Capacity loss for the case that the desired user is located at the center of the interferer cluster, i.e. ($s = s_c$), plotted for $\forall s_1$ (i.e. $\forall \theta_1$. Cluster Δs_c is set such as to fix $\Delta\theta_c = 3°$.

[5] J. S. Kwak, J. G. Andrews, and A. Lozano, "MIMO capacity in correlated interference-limited channels," in *IEEE International Symposium on Information Theory*, pp. 106–110, June 2007.

[6] A. Forenza, D. Love, and R. Heath, "Simplified spatial correlation models for clustered MIMO channels with different array configurations," *IEEE Transactions on Vehicular Technology*, vol. 56, pp. 1924–1934, July 2007.

[7] X. Gao, F. Tufvesson, and O. Edfors, "Massive MIMO channels - measurements and models," in *Asilomar Conference on Signals, Systems and Computers*, pp. 280–284, Nov. 2013.

[8] J. Lv, Y. Lu, Y. Wang, H. Zhao, and C. Y. Han, "Antenna spacing effect on indoor MIMO channel capacity," in *2005 Asia-Pacific Microwave Conference Proceedings*, vol. 3, Dec. 2005.

[9] H. Xu, D. Chizhik, H. Huang, and R. Valenzuela, "A generalized space-time multiple-input multiple-output (MIMO) channel model," *IEEE Transactions on Wireless Communications*, vol. 3, pp. 966–975, May 2004.

[10] A. Manikas, A. Alexiou, and H. R. Karimi, "Comparison of the ultimate direction-finding capabilities of a number of planar array geometries," *IEE Proceedings: Radar, Sonar and Navigation*, vol. 144, pp. 321–329, Dec. 1997.

[11] A. Manikas, *Differential geometry in array processing*. Imperial College Press, 2004.

[12] A. A. Abouda, H. M. El-Sallabi, and S. G. Haggman, "Impact of antenna array geometry on mimo channel eigenvalues," in *2005 IEEE 16th International Symposium on Personal, Indoor and Mobile Radio Communications*, vol. 1, pp. 568–572, Sept. 2005.

[13] P. Chandhar, D. Danev, and E. G. Larsson, "On ergodic rates and optimal array geometry in line-of-sight massive mimo," in *2016 IEEE 17th International Workshop on Signal Processing Advances in Wireless Communications (SPAWC)*, pp. 1–6, July 2016.

[14] W. Tan, S. Jin, J. Wang, and Y. Huang, "Achievable sum-rate analysis for massive mimo systems with different array configurations," in *2015 IEEE Wireless Communications and Networking Conference (WCNC)*, pp. 316–321, Mar. 2015.